Small Angle Neutron Scattering Study of PbS Quantum Dots Synthetic Routes via Sol-Gel

M. PIÑERO*

Dpto. Física Aplicada, C.A.S.E.M., Universidad de Cádiz, 11510 Puerto Real, Cádiz, Spain

manolo.piniero@uca.es

N. DE LA ROSA-FOX, R. ERCE-MONTILLA AND L. ESQUIVIAS

Dpto. de Física de la Materia Condensada, Facultad de Ciencias, Universidad de Cádiz, 11510 Puerto Real, Cádiz, Spain

Abstract. SiO_2 organically modified silicate (ormosil) gels doped with different concentration of PbS quantum dots ranging from 0.5 to 4 wt%, were synthesised via sol-gel. The synthesis implied a process including the hydrolysis assisted with high power ultrasounds of tetramethylorthosilicate (TMOS) mixed with polydimethylsiloxane (PDMS). Colloidal dispersions of PbS embedded in sono-ormosil matrices were obtained by using two different control size agents: the complexing ethylenediamintetraacetic acid (EDTA), and the surface modifier mercaptopropyltrymethoxysilane (MPTMS). Small Angle Neutron Scattering (SANS) study of these samples revealed some differences in the resulting PbS size and size distribution for the materials obtained by the two methods above. The data analysis using a two-correlation function combined with Percus–Yevick hard-spheres model, indicates the existence of PbS core-shell aggregates of 15–75 nm diameter size, homogeneously distributed in a microporous matrix with mean pore size of 0.5 nm.

Keywords: sonogel, ormosil, PbS nanocrystals, SANS

1. Introduction

Semiconductor nanocrystals embedded in gel matrices are materials of great interest due to their enhanced non-linear optical properties. A lot of work is devoted to this subject with the aim of approximate the fabrication of size-controlled quantum dots exhibiting the massive change optical properties as the Bohr's radius is attained [1, 2].

One of the quantum dots (QDs) material where extensively research has been dedicated recently [3–5] is PbS, because its bulk absorption edge is located at around 3300 nm, and it can be shifted by more than 2000 nm towards the region of the telecommunication wavelengths [6].

The sol-gel method offers a relatively easy way for preparing such materials. Moreover, the fabrication of new hybrid organic-inorganic materials named ormosil with promising mechanical properties as well as optical quality, have attracted much interest for preparing the matrices for QDs [7]. In addition, the use of high-power ultrasounds at the sol stage enhances the homogeneity at microstructure in the final material [8]. Previous investigations by other authors [9] into this kind of materials, using scattering techniques, signalled the existence of influences on the structure factor due to polymer crosslinking. In that case, this also indicates the probability of the formation of supermolecular structures [10].

In this study we compare two similar ways for synthesising PbS QDs into rigid transparent SiO_2-PDMS

---

*To whom all correspondence should be addressed.

sono-ormosils, for non-linear optical applications. One of them utilises EDTA to complex lead ions, thus avoiding precipitation of the sulphur, while the other one makes use of MPTMS, as surface capping agent (SCA), thus allowing the formation of stabilized PbS colloidal dispersion. Structure analysis was determined by Small Angle Neutron Scattering (SANS), revealing the existence of residual elastic strains in the network due to polymer cross-links and crystal sizes in the confinement regime.

2. Experimental

We used silanol-terminated PDMS with quoted average molecular weigt of 400–700, and TMOS, for preparing hybrid organic-inorganic host matrices. Using ultrasonic irradiation to form "sono-ormosils" shortened the chemical reactions between both organic and inorganic precursors [11]. In order to ensure the homogeneous incorporation of PDMS chains into the silica inorganic network, a two-step hydrolysis was used and described as follows:

TMOS was first partially hydrolysed with HNO_3 catalyst in a molar ratio of $TMOS:H_2O:HNO_3$ of 1:0.84:0.026. The organic polymer PDMS was added in a molar ratio TMOS:DMS of 1:0.19, where the organic fraction has been expressed as a function of the dimethyl-siloxane monomer, DMS. At this step, the resulting solution (sol A) received 320 $J \cdot cm^{-3}$ ultrasounds energy, and was translucide due to sub-micro or even nanophase separation, as a result of thermodynamic incompatibility between the organic and inorganic precursors. It was kept at 50°C for 24 hours and, along this time, it evolved into transparent solution suspecting that covalent bonds have been formed between silanol groups of PDMS chains and the inorganic constituent.

Hydrolysis of sol A was completed subsequently with a molar ratio $TMOS:H_2O:HNO_3$ of 1:3.36:0.0015, with 500 $J \cdot cm^{-3}$ of ultrasound energy. Transparent homogeneous sol obtained was suitable for doping. From this point, we proceeded to mix lead nitrate or lead acetate and TAA inside the organic-inorganic silica sol, to get 0.5, 1, 2, and 4 wt% PbS nanocrystals doped ormosils.

In route I, EDTA was added for chelating Pb^{2+} ions prior to sulphur addition, to prevent growth of PbS particles and further precipitation. Here, the molar ratio of $TMOS:H_2O:PDMS:HNO_3:EDTA$ was 1:4.2:0.19:0.026:0.0002, respectively. We pre-

Table 1. Molar ratios respect to TMOS of the reactive precursors used in the preparation of PbS-ormosils. The code sample is referred as XRY, X being the nominal PbS wt% and Y the MPTMS/Pb molar ratio multiplied by a factor of 10^3.

Sample	$PbAc_2$	MPTMS x $(10)^{-3}$	TAA	NH_3
Matrix IIA	–	41.6	–	0.06
Matrix IIB	–	–	–	0.02
0.5R16	1.35	20.8	1.8	0.056
0.5R32	1.35	41.6	1.8	0.057
0.5R64	1.35	83.2	1.8	0.057
1R10	2.7	26.0	3.6	0.044
4R5	10.8	52.0	14.4	0.047

pared PbSEDTA1 sample with a molar ratio $TMOS:Pb(NO_3)_2:TAA$ of 1:0.003:0.012.

In route II, aggregation and subsequent precipitation of lead sulfide was help it by using MPTMS which acts as a SCA in the small PbS particles, thus promoting a highly dispersed dot population. The molar ratios used are indicated in Table 1. The gel transition was accelerated by adding ammonia methanolic solution. By this way, yellow coloured gels were obtained which turn progressively into orange, red, brown and black coloured transparent gels.

All of the samples were heat-treated up to 100°C at 1°C/min for 3 hours in N_2 atmosphere, to avoid decomposition of PbS to form the corresponding oxide PbO.

SANS measurements were made at room temperature on the V4 workstation at the HMI, Berlin, using a neutron wavelength of 6.02 Å, at three detector distances 1, 4 and 16 m to cover a q-range from 0.036 to 3.6 nm^{-1}. Data were corrected using software package available at HMI [12]. Normalized intensities were analysed by calculating with the aid of suitable models, the form factor $P(q)$ and the structure factor $S(q)$, according to $I(q) = (\Delta\rho)^2 N P(q) S(q)$, N being the number density and $\Delta\rho$ the contrast difference between the scatters and the surrounding media.

3. Results and Discussion

Figure 1(a) shows the SANS curves of three sono-ormosil matrices with variation in the SCA and catalyst content (Table 1). Scattering curve from matrix I, have not discernable compositional fluctuations at low-q, signaling that there is no appreciable chemical
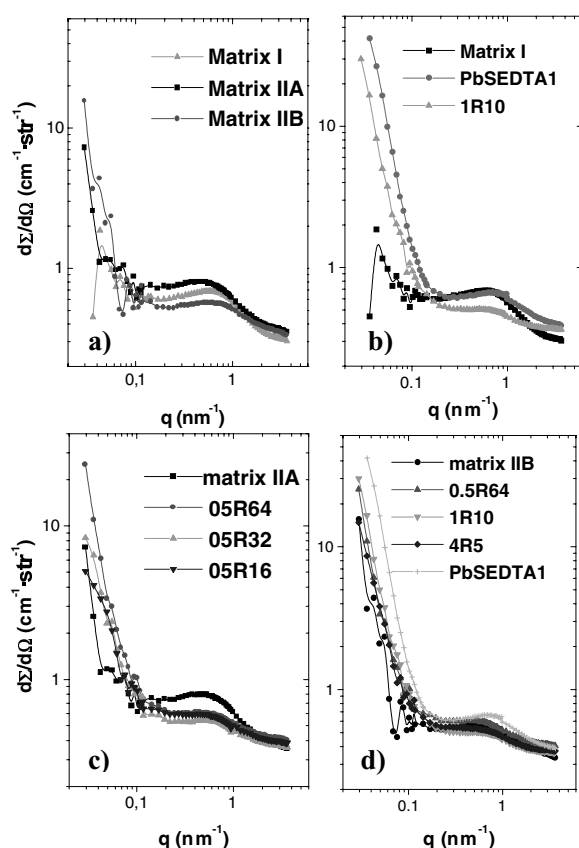
Figure 1. SANS patterns from: (a) sono-ormosil matrices: I (acid catalyst), IIA (SCA and pH increased), and IIB (pH increased). Differences in scattering at low-q are attributed to the existence of polymer cross-linking. (b) PbSEDTA1 and 1R10 samples. The corresponding matrix I SANS curve is now depicted to elucidate the scattering source in both doped sono-ormosils above, at low-q; (c) matrix IIA,05R16, 05R32 and 05R64 doped samples. (d) matrix IIB, 05R64,1R10,4R5 and PbSEDTA1 samples. (Continuous line is a guide for the eye in all cases.)

differences inside the hybrid organic-inorganic network. The most relevant feature observed for matrices IIA and IIB scattering curves is the strong increase in intensity at low-q, with a crossover at 0.1 nm^{-1}. These samples contain little amounts of catalyst base, differing respect to matrix I, which was only prepared under acidic conditions. This fact induces the apparition of constraints in the forming network of IIA and IIB, and suggests that the scattering increase at low-q must be due to local heterogeneities due to polymer cross-links, which are formed very rapidly provoking gelation. Also, the effect of the addition of MPTMS (IIA) produces modifications at a microstructural level inducing the small differences observed at medium q-range.

In all cases, a flat region with a broad shoulder developing at 0.6 nm^{-1} is observed. This is characteristic of well-shaped scatters homogeneously distributed, and must be produced by the fine porosity of the matrix [13]. Some incoherent scattering due to the hydrogen of the polymer chains is observed at high-q, this is the reason why Porod-like behaviour is not observable.

Figure 1(b) shows SANS curves from 1% doped samples and matrix I. It is apparent the increase of the intensity at low-q in the case of the doped samples. This clearly evidences the formation of PbS nanocrystals, of different sizes depending on the followed synthetic route, I or II.

Figure 1(c) shows SANS curves for samples based in the matrix IIA. The most relevant difference is the increase of intensity at low-q due to the presence of PbS nanocrystals capped with the MPTMS molecules and the porosity shoulder at 0.6 nm^{-1}. The intensity increases as the SCA content increase.

Figure 1(d), shows SANS curves for the outlined samples. As can be observed there are no significant changes, this means that the matrix microstructure as well as PbS particle size are well stabilised. However, appreciable scattering difference is detected in PbSEDTA1 sample, due to the different complexing agent behaviour to get control size and stabilisation of the PbS precipitates.

By assuming a random two-phase system for describing the PbS doped sono-ormosils [14], we proposed a two-correlation length model for the scattering form factor from the Debye-Bueche relationship:

$$P(q) = \frac{A_1}{\left(1 + q^2 a_1^2\right)^2} + A_2 e^{-\frac{q^2 a_2^2}{4}} \qquad (1)$$

where a_1 and a_2 represent the correlation lengths for the medium and short-range fluctuations, respectively. The coefficients A_1 and A_2 are related with the volume fraction of each phase.

On the other hand, the structure factor $S(q)$ was evaluated assuming the Percus-Yevick hard-sphere model, and using the expression of Ashcroft and Lekner [15]. This approach of the SANS patterns involves the existence of a depleted region around the PbS crystals, where the growth of another crystal is inhibited [16].

Figure 2 shows a comparison between the experimental and calculated SANS fit to Eq. (1). In the high-q region the model does not accounts due to the incoherent scattering contribution, in the absence of which,
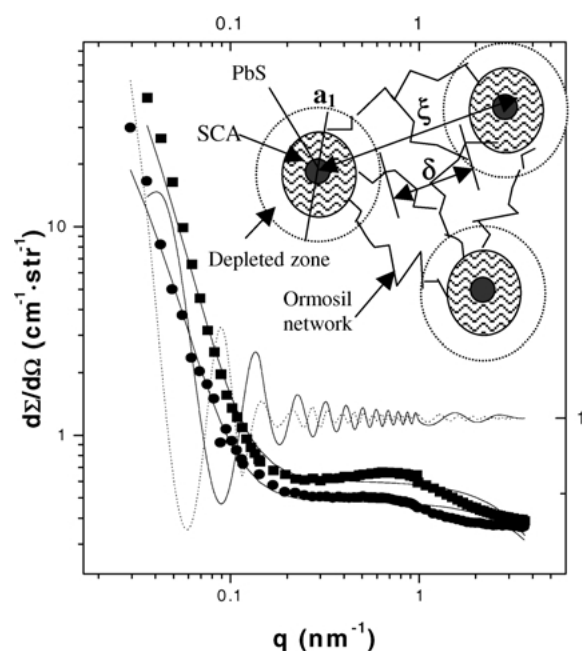
Figure 2. Decovolution of the experimental (dotted line) SANS patterns of PbSEDTA1 (■) and 1R10 (●) samples, calculated by using a sacttering factor from a two-correlation function combined with Percus-Yevick hard-spheres model. The divergence of the fit (continuous line) at high-q is due to the incoherent scattering contribution from H in the polymer chains. The structure factor from both the PbSEDTA1 sample (continuous line) and the1R10 one (dotted line) are also depicted and exhibit oscillation around unity. Inset shows the proposed structure model for PbS doped sono-ormosil.

the knee of the fit curves at $q = 2$ nm^{-1} will shift to smaller values accounting for bigger scatters.

The results of the fitting are shown in Table 2. The long-range correlation length a_1 increases with PbS and SCA concentration. It is reasonable to assume this length as the mean diameter size of the surface capped PbS particle, which includes a depleted region surrounding the crystal. This geometry explains well the high increase of a_1 value observed for 05R64,

Table 2. Fit parameters from two-correlation model and Percus-Yevick Hard-Sphere diameter.

Sample	a_1 (nm)	A_1	a_2 (nm)	ξ (nm)
PbSEDTA1	41.08	310.68	0.43	68.74
0.5R16	21.41	7.15	0.41	70.32
0.5R32	21.89	9.36	0.39	93.71
0.5R64	74.67	737.79	0.43	138.35
1R10	35.10	78.34	0.36	104.66
4R5	42.71	96.67	0.40	167.32

comparing to that from 05R32, which is almost similar to both 05R10 and 05R16 samples. An increase of A_1 coefficcients is observed as PbS and SCA concentration increase. This corroborates the assumption that the intensity at low-q values is predominantly due to scattering from MPTMS surface capped PbS nanoparticles. It is not possible to discern if the short range correlation length a_2 does exhibits a significant trend. However they are in agreement with the mean pore diameter attributed to microporous phase by N$_2$-adsorption techniques [13].

The coefficients A_2 (not shown) are similar for all of the analysed samples, accounting for the stability of the sono-ormosil matrix at the fine porosity level.

Fit values of the hard-sphere diameter, ξ, agrees well with the supposed scattering center structure. In all cases the volume fraction, η, was around 0.15. A suitable geometric model will set up, yielding the PbS-doped sono-ormosil structure as shown in the inset of Fig. 2. In this model, the scattering centers are composed of a spherical core of PbS nanocrystal surrounded by the SCA molecules, which link to the polymer network in the transition zone. The diameter of the whole scattering center accounts for the correlation length a_1, and the hard-sphere diameter, ξ, for the distance between centers of the aggregates. The distribution of them in the ormosil matrix can be approximated by $\delta = (\xi - a_1)$, and should represents the correlation distance between the scattering centers with diameter a_1. In order to illustrate this structural model, a transmission electronic microscopy image of sample 1R10 is shown in Fig. 3. PbS nanocrystals for this sample
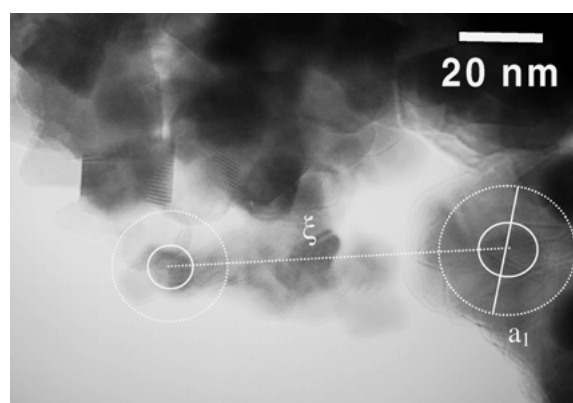
Figure 3. High resolution transmission electronic microscopy of 1R10 sample showing the size and distribution of PbS nanocrystals embedded in the amorphous polymer matrix according to the proposed structural model.

present mean size of 7.5 nm at the core of the aggregates, which appear randomly distributed into the ormosil matrix. Also, in order to clarify the correspondance between TEM image and the proposed structural model, this has been illustrated on the image showing the correlation between two aggregates. The inner circle representing the PbS nanocrystal surrounded by SCA, and the outer circle is an approximation of the depleted region.

4. Conclusions

The SANS results presented in this paper suggest the existence of a two phase systems, constituted by homogenous dipersions of PbS particles with controlled-size and a microporosity uniformly distributed in the sono-ormosil matrix.

The short-range correlation length represents the microporosity of the sono-ormosil. The hard-sphere diameter combined with the evaluated long-range correlation length gives rise to a description of the microstructure of this kind of materials. SCA molecules and a depleted region where crystal growth is inhibited, forming a core-shell aggregate surround them.

Acknowledgments

References

1. A.I.L. Efros and A.L. Efros, Sov. Phys. Semicond. **16**, 722 (1982).
2. L.E. Brus, J. Phys. Chem. **90**, 2555 (1986).
3. A. Martucci, P. Innocenzi, J. Fick, and J.D. Mackenzie, J. Non-Cryst. Solids **244**, 55 (1999).
4. F. Del Monte, Y. Xu, and J. Mackenzie, J. Non-Cryst. Solids **17**, 37 (2000).
5. S. Chen, W. Liu, and L.Yu, J. Mater. Res. **14**(5), 2147 (1999).
6. R. Jain and R. Lind, J. Opt. Soc. Am. **73**(5), 647 (1983).
7. J.D. Mackenzie, J. Sol-Gel Sci.Tech. **2**, 81 (1994).
8. T. Iwamoto and J. Mackenzie, J. Sol-Gel Sci.Tech. **4**, 141 (1995).
9. E. Geissler, F. Horkay, A. Hecht, C. Rochas, P. Lindner, C. Bourgaux, and G. Couarraze, Polymer **38**(1), 15 (1997).
10. S. Mallam, A. Hecht, E. Geissler, and P. Prevost, J. Chem. Phys. **91**, 6447 (1989).
11. K. Morita, Y. Hu, and J.D. Mackenzie, J. Sol-Gel Sci. Tech. **3**, 109 (1994).
12. U. Keiderling, Physica B **234–236**, 1111 (1997).
13. R. Erce-Montilla, M. Piñero, A. Santos, N. de la Rosa-Fox, and L. Esquivias, J. Mat. Res. **16**, 2572 (2001).
14. N. De la Rosa-Fox, R. Erce-Montilla, M. Piñero, and L. Esquivias, Opt. Mater., in press (2002).
15. N. Ashcroft and J. Lekner, Phys. Rev. **145**, 83 (1966).
16. G. Banfi, V. Degiorgio, and B. Sepeit, J. Appl. Phys. **74**, 6925 (1993).